FULL PAPER

Optoelectronic Devices

ADVANCED
FUNCTIONA
MATERIALS
www.afm-journal.d

Check for
updates

PdSe$_2$ Multilayer on Germanium Nanocones Array with Light Trapping Effect for Sensitive Infrared Photodetector and Image Sensing Application

Lin-Bao Luo, Di Wang, Chao Xie,* Ji-Gang Hu,* Xing-Yuan Zhao, and Feng-Xia Liang*

In this study, a sensitive infrared photodetector (IRPD) composed of a germanium nanocones (GeNCs) array and PdSe$_2$ multilayer is presented, which is obtained by a straightforward selenization approach. The as-assembled PdSe$_2$/GeNCs hybrid heterojunction exhibits obvious photovoltaic behavior to 1550 nm illumination, which renders the IRPD a self-driven device without external power supply. Further device analysis reveals that the PdSe$_2$/GeNCs hybrid based IRPD exhibits high sensitivity to 1350, 1550, and 1650 nm illumination with excellent stability and reproducibility. The responsivity and external quantum efficiency is as high as 530.2 mA W^{-1} and 42.4%, respectively. Such a relatively good device performance is related to the strong light trapping effect of GeNCs array, according to the theoretical simulation based on finite-difference time-domain. It is also found that the IRPD shows an abnormal sensitivity to IR illumination with a wavelength of 2200 nm. Finally, the present individual IRPD can also record the simple "F" image produced by 1550 nm, suggesting the promising application of the PdSe$_2$/GeNCs hybrid device in future infrared optoelectronic systems.

1. Introduction

Graphene, a monolayer of carbon atoms arranged in a closely packed 2D honeycomb fashion, has recently attracted worldwide research interest owning to its wideranging application in various fields, such as optoelectronic devices,[1–3] energy conversion, and storage devices,[4,5] chemical and biological sensors,[6,7] and high-frequency electronic and optical devices.[8–10] While the past decade has witnessed a huge progress in this field, it is undeniable that there remain grand challenges and the practical application of graphene devices is greatly hindered by the absence of inherent bandgap and short photocarrier lifetime.[11,12] Such dilemma has prompted the materials

scientists to search for alternative 2D materials, such as black phosphorus,[13] arsenene,[14,15] antimonene,[16,17] black arsenic phosphorus,[18] silicone,[19] and layered transition metal dichalcogenides (TMDs, such as MoS$_2$,[20] MoSe$_2$,[21] and MoTe$_2$[22] etc.) with a general formula of MX$_2$. Up to now, a number of synthetic strategies including mechanical exfoliation, liquid phase exfoliation, and chemical vapor deposition have been developed to fabricate 2D materials.[23] Like graphene, the atomically thin 2D materials obtained by the above methods have demonstrated various distinctive properties in terms of adjustable bandgap, defect-free surface structure, excellent mechanical flexibility, and high electron/hole motilities which can never be observed in their 3D bulk or thin-film counterparts.[24]

In addition to the above 2D materials, PtSe$_2$ as a representative of the newly discovered group-10 TMDs has come under spotlight owing to its excellent ambient stability and adjustable bandgap ranging from zero for multilayer to 1.2 eV for monolayer.[25,26] This thickness-dependent bandgap greatly facilitates the fabrication of high mobility transistor and high-performance photodetectors working in infrared light region,[27,28] which are crucial components for application in various fields, such as missile detection, light vision, target tracking, and military surveillance. For instance, Chai's group achieved a few-layer PtSe$_2$ based field-effect transistor.[29] Such a device exhibited a high room-temperature mobility of 210 cm^2 V^{-1} s^{-1}, which is comparable to that of black phosphorus. By direct selenization of Pt film, Wang and co-workers achieved the epitaxial growth of high-quality, monolayer PtSe$_2$, which demonstrated excellent catalytic activity in methylene-blue photodegradation experiment.[30] Moreover, Zeng et al. reported on the large-area fabrication of PtSe$_2$ through a straightforward selenization method. By combing GaAs with the vertically aligned PtSe$_2$ multilayer, a highly sensitive photodetector with a broadband sensitivity from deep ultraviolet to infrared light was obtained. In spite of great progresses achieved in PtSe$_2$ based electrical and optoelectronic devices, relatively few work has been reported on PdSe$_2$, which is equally important member of group-10 TMDs.[31,32] Here, in this work, we report on the development of a sensitive infrared photodetector (IRPD) consisted of multilayered PdSe$_2$/Ge nanocone (GeNC) arrays.

Dr. L.-B. Luo, D. Wang, Dr. C. Xie, Dr. J.-G. Hu
School of Electronic Science and Applied Physics
Hefei University of Technology
Hefei 230009, China
E-mail: chao.xie@hfut.edu.cn; hujigang@hfut.edu.cn
X.-Y. Zhao, Dr. F.-X. Liang
School of Materials Science and Engineering
Hefei University of Technology
Hefei 230009, China
E-mail: fxliang@hfut.edu.cn

Thanks to the strong light trapping effect, the as-assembled $PdSe_2$/GeNC arrays device exhibits pronounced photovoltaic characteristics under infrared light illumination, which allows the heterojunction device to detect IR without external power supply. Further device analysis reveals that the $PdSe_2$/GeNC arrays device exhibits obvious sensitivity to repeatable 1350, 1550, 1650, and even 2200 nm illumination with good reproducibility. Specifically, the responsivity is estimated to be 530.2 mA W^{-1}, which is much better than other group-10 TMDs based device including $PtSe_2$/GaAs[26] and $PdSe_2$/Si.[33] What is more, the specific detectivity under 1550 nm illumination is 1.45×10^{11} Jones, respectively. Such a value is higher than most of the germanium based devices ever reported. In addition, the device also has a very fast response speed, with rise time/decay time of 21.2 and 40.2 µs, respectively. It is also observed that the $PdSe_2$/GeNC can reliably record the simple and infrared light image. The above result suggests the present $PdSe_2$/GeNC arrays heterojunction device will exhibit great potential in the future optoelectronic devices and systems.

2. Results and Discussion

The IRPD is structurally composed of free-standing germanium nanocones (GeNCs) array coated with a layer of $PdSe_2$ film, which was characterized by waved Pd–Se layers held together by van der Waals force as illustrated in **Figure 1**a. In this study, the periodic GeNCs array was obtained by noble metal assisted HF etching method, during which polystyrene (PS) sphere lithography was used to define the size of the Ge structures. Figure 1b shows a cross-section scanning electron microscopy (SEM) image of the GeNCs array, with a height of 4 µm and a diameter of 500 nm, respectively. Figure S1 in the Supporting Information shows a typical camera picture

of both Pd and $PdSe_2$ films. It is clear that the color changed from orchid to light sky blue after selenization. By studying the SEM image of the as-selenized $PdSe_2$ in Figure 1c, one can easily find that the $PdSe_2$ has relatively smooth surface with good continuity. According to further atomic force microscopy (AFM) image shown in Figure 1d, the $PdSe_2$ has a thickness of around 33 nm. Raman spectra of $PdSe_2$ nanofilm in Figure 1c show four obvious peaks at ≈144, ≈206, ≈222, and ≈256 cm^{-1} due to A_g^1, A_g^2, B_g^1, and A_g^3, respectively.[33] The three peaks at the relatively low Raman shift are related to the movement modes of Se atoms, whereas the strongest peak corresponds to the relative motion between Se and Pd atoms. The insert pattern is X-ray diffraction (XRD) analysis of the $PdSe_2$ sample, we found that the prepared $PdSe_2$ possesses pentagonal structure with $a = 5.735$, $b = 5.858$, and $c = 7.672$ Å, which is close to the values of standard card (PDF#11-0453) and previous work.[34] As a matter of fact, the chemical composition of $PdSe_2$ was also confirmed by X-ray photoemission spectroscopy in Figure S2 in the Supporting Information, and energy-dispersive X-ray spectroscopy (EDS), in which the atomic ratio of Pd:Se is determined approximately to be 1:2 (Figure 1f).

Figure 2a shows the current–voltage (I–V) curve of a representative $PdSe_2$/GeNC array device measured in the dark. Obviously, the device shows a rectifying behavior with a weak rectification ratio of ≈5 at ± 1 V. Seeing that Ohmic contact was formed for both Ag/$PdSe_2$/Ag and In/Ga–Ge–In/Ga structures (Figure S3, Supporting Information), the above rectifying behavior can be exclusively attributed to $PdSe_2$/GeNCs array heterojunction. Interestingly, once shined by 1550 nm near infrared (NIR) light, the hybrid structure array based device will display obvious photovoltaic characteristics, with an open-circuit voltage (V_{OC}) of 0.13 V and a short-circuit current (I_{SC}) of 0.41 mA at 4.32 mW cm^{-2} illumination. Such an obvious photovoltaic behavior is relatively weak and the correspondingly
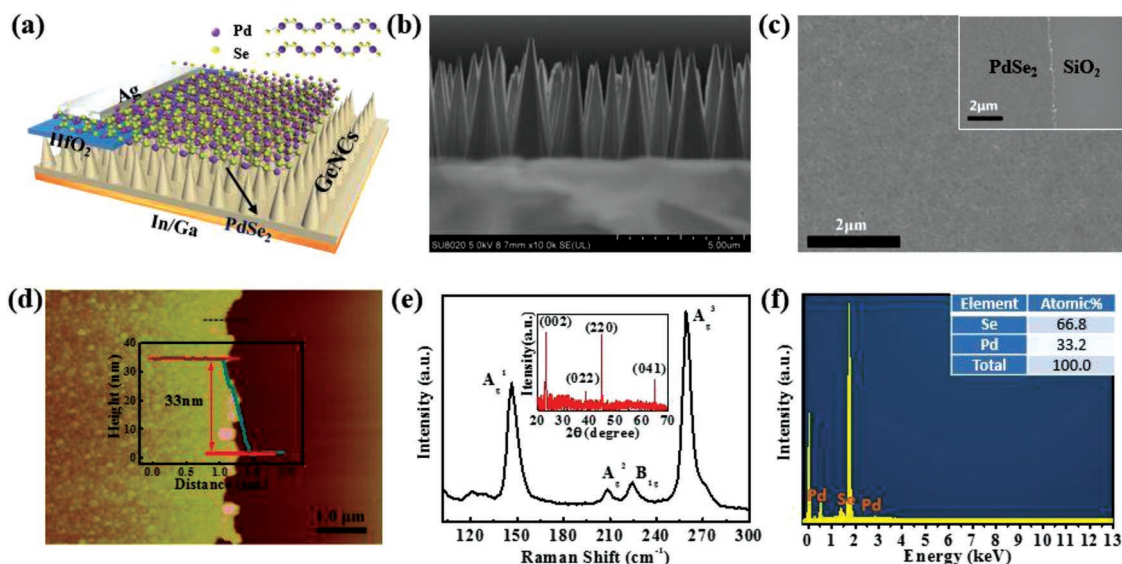

Figure 1. a) Schematic illustration of the $PdSe_2$/GeNC array heterojunction photodetector. b) A typical cross-sectional SEM image of GeNC array. c) SEM image of the $PdSe_2$ layer, the inset shows SEM image of an as-prepared $PdSe_2$ layer on a SiO_2 substrate. d) AFM image of the $PdSe_2$ layer, the inset shows the height profile. e) Raman spectra of the $PdSe_2$ film, the inset shows XRD pattern of $PdSe_2$ film. f) EDS analysis of the $PdSe_2$ sample.
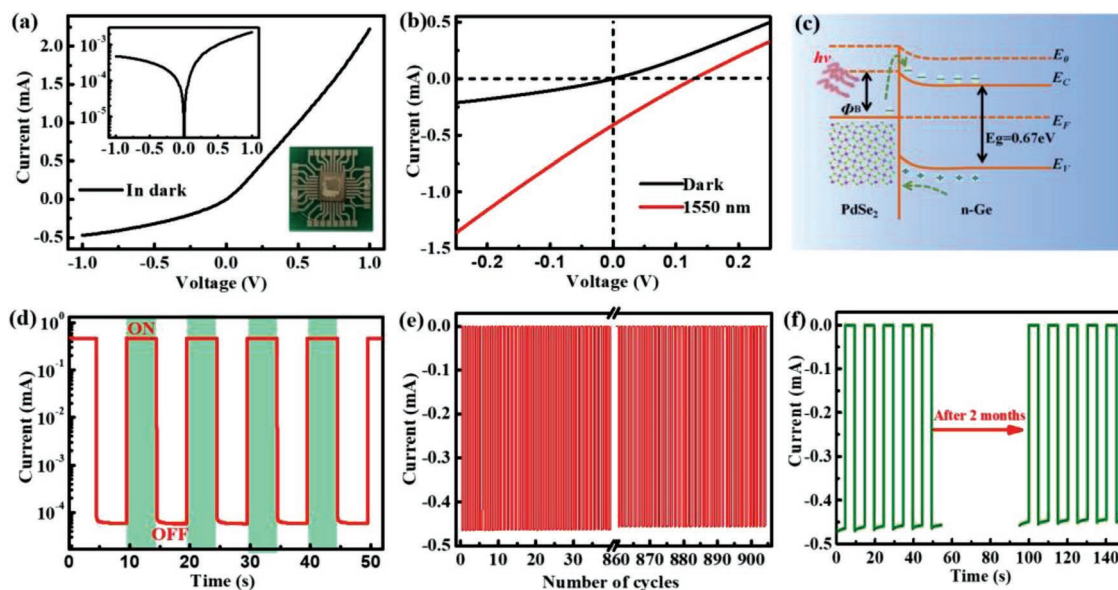
Figure 2. a) $I–V$ curves of the PdSe$_2$/GeNC array heterojunction in darkness, the inset shows a digital camera picture of the device. b) $I–V$ characteristics of the device in the dark and illuminated with 1550 nm light (4.32 mW cm^{-2}). c) The energy band diagram under IR illumination. d) Photoresponse of the IRPD under 1550 nm light illumination (4.32 mW cm^{-2}) at zero bias. e) Photoresponse of the IRPD for about 900 cycles of operation. f) Photoresponse of the IRPD before and after 2 months storage in ambient condition.

power conversion efficiency is low (less than 1%). However, similar to what was observed in graphene/semiconductor heterojunction devices,[35] it can allow the photodetector as a self-driven device. This photoelectric behavior actually can be interpreted by the energy band diagram shown in Figure 2c. A built-in electric field at the PdSe$_2$/GeNCs interface was formed due to their difference in work function. (The work function is 4.37 eV for Ge and 5.49 eV for PdSe$_2$ multilayer, respectively, please see the Figure S4 in the Supporting Information.) When shined by IR light, the electric field will separate the photogenerated electron–hole pairs, leading to movement of free electrons and holes, and subsequently the formation of photocurrent in circuit.[36] Figure 2d exhibits the time-dependent photoresponse under periodically switched 1550 nm at zero bias. Obviously, our device is highly sensitive to the incident NIR light, with a repeatable and stable I_{light}/I_{dark} ratio of ≈7×10^3. It is also found that the curve has very steep rise and fall edges, signifying fast separation of electrons–holes pairs by electric field. Notably, the curve can keep nearly unchanged after 900 cycles of illumination and even after 2 months storage in ambient condition. This excellent ambient stability is obviously due to the superior stability of the PdSe$_2$ multilayer (Figure S5, Supporting Information).

The photovoltaic behavior of the PdSe$_2$/GeNC array heterojunction device is highly dependent on the incident IR intensity. **Figure 3**a exhibits the $I–V$ characteristics of the heterojunction device under IR light with light intensity ranging from 5 μW cm^{-2} to 4.32 mW cm^{-2}. It can be found that the photocurrent increased gradually with increasing incident IR intensity, because of increased population of photoexcited charge carriers under higher intensity. Similar evolution was also observed on photovoltage, which is found to increase when the light intensity increases from 5 μW cm^{-2} to 3 mW cm^{-2}. Nonetheless, further increase in intensity leads to a saturation

in photovoltage (Figure 3b). To quantitatively evaluate the relationship between photocurrent and light intensity, the photoresponse of the IRPD under different light intensities is explored (Figure 3c). Figure 3d shows the photocurrent at different light intensities. Obviously, this relationship can be described by a power law: $I_{ph} \propto P^\theta$, where θ is an exponent and P is the intensity. Fitting the curve leads to two different exponent values: $\theta = 0.89$ for the weak intensity region and $\theta = 0.63$ for the strong intensity region. The fitting results shows that the recombination loss is relatively weaker at lower light intensity, but will become stronger at higher light intensity due to the higher density of the photogenerated carriers as well as the existence of some trap states between the Fermi level and the conduction band edge.

Further device performance analysis finds that the I_{light}/I_{dark} ratio of the IRPD increases gradually with increasing incident light intensity. Specifically, it can achieve a maximum value of 7×10^3 when the light intensity is as high as 4.32 mW cm^{-2} (Figure 3e). By using the following Equation (1), both external quantum efficiency (EQE) and the responsivity (R) were then calculated[25,37]

$$R\left(\mathrm{AW}^{-1}\right) = \frac{I_{light} - I_{dark}}{P_\lambda S} = \mathrm{EQE}\left(\frac{q\lambda}{hc}\right)G \tag{1}$$

where S, P_λ, I_{light}, I_{dark}, h, c, λ, and G are the effective illuminated area, the incident 1550 nm light intensity, the photocurrent, the current in the dark, the Planck's constant, the light speed, and the light wavelength, respectively. G is unity in that an internal gain mechanism is nonexistent for the common photodiodes. Based on these values, R and EQE at different IR intensities were calculated and shown in Figure 3f. Note that both EQE and R decrease with increasing light intensity, owing to intensified recombination activity at higher light
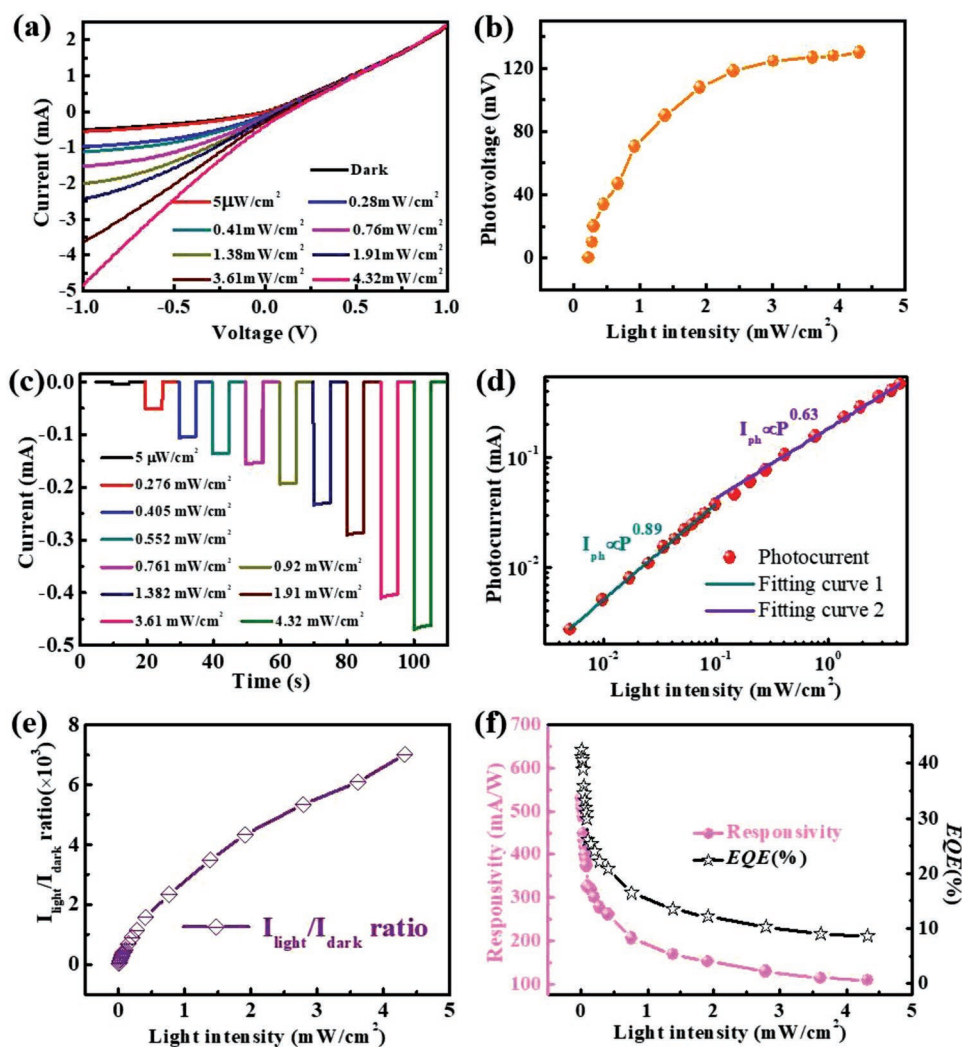
**ADVANCED
SCIENCE NEWS**

www.advancedsciencenews.com

**ADVANCED
FUNCTIONAL
MATERIALS**

www.afm-journal.de

Figure 3. a) I–V curves of the heterojunction device under 1550 nm light with varied light intensities. b) Relationship between photovoltage of the device and incident light intensity. c) Photoresponse of the heterojunction device under 1550 nm light with varied light intensities at zero bias. d) The fitting curve of both photocurrent and light intensity. e) The dependence of I_{light}/I_{dark} ratio on the light intensity at zero bias. f) Responsivity and EQE as functions of the incident light intensity under 1550 nm light.

intensity.[38] In light of this, a maximum R and EQE are calculated to be 530.2 mA W^{-1} and 42.4% at a low light intensity of 5 μW cm^{-2}. (Please see the detailed calculation process in the Supporting Information.) The responsivity is much better than other group-10 TMDs based device including PtSe$_2$/GaAs[26] and PdSe$_2$/Si.[33]

In addition to the obvious sensitivity at 1550 nm, the IRPD also exhibits stable response to other IR illumination. **Figure 4**a shows the photoresponse of IRPD when shined by 1300, 1550, and 1650 nm with the same intensity (4.32 mW cm^{-2}). It is clear that the device can be readily switched between high- and low-resistance states for all the three wavelengths. Comparatively, the photocurrent under 1550 nm is the highest, which is related to the inherent bandgap of germanium. The I_{light}/I_{dark} ratio and responsivity at different light intensities for three different wavelength were calculated in Figure 4b,c, respectively, which show similar evolution as for the 1550 nm. Another finding that deserves further discussion is that the present

IRPD is even sensitive to IR illumination with wavelength of 2200 nm. Figure 4d records the photoresponse curve shined by 2200 nm IR with a relatively strong intensity ($\approx$80.2 μW cm^{-2}). It is seen that the device shows repeatable switching between on/off states. This finding is abnormal because the PdSe$_2$ multilayer possess typical metallic behavior when the thickness is larger than 20 nm, and there is no evidence for the opening of bandgap of PdSe$_2$ due to incorporating interstitial Se atoms into van der layer (Figure S6, Supporting Information).[33] Although the detailed reason for this finding is still unknown to us, similar photoresponse in infrared light has been previously reported in semimetal graphene-based photodetectors, in which operational wavelengths of 1.55,[39] 2.4,[40] and even 3.2 μm[41] were realized.

Moreover, the present IRPD device was capable of detecting high-frequency pulsed IR light with good reproducibility. **Figure 5**a plots the photoresponse when illuminated by 1550 nm irradiation with frequency of both 1 and 20 kHz. It is clear that
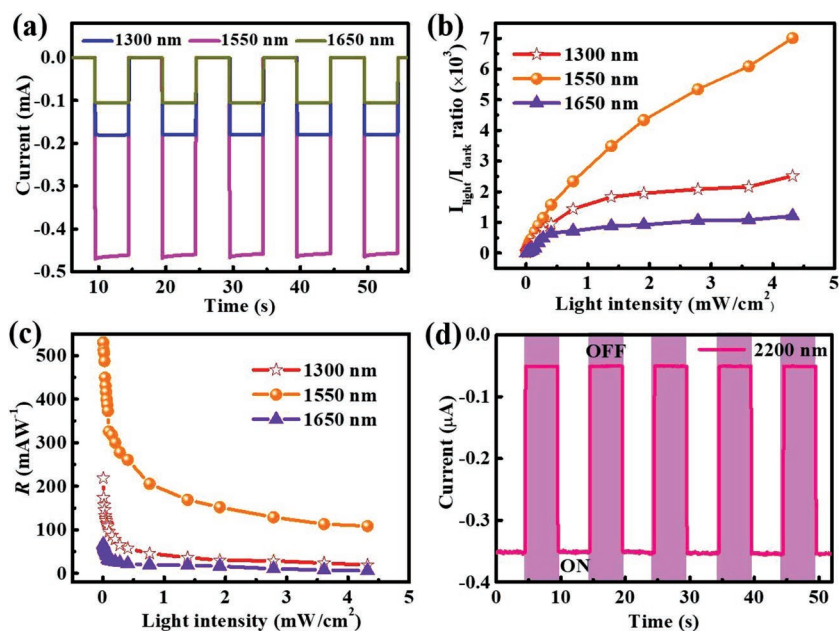
Figure 4. a) Time-dependent photoresponse of the device under illumination of different infrared light (4.32 mW cm^{-2}) at zero bias. b) I_{light}/I_{dark} ratios as a function of the light intensity for different wavelength. c) The relationship between the responsivity and the light intensity. d) Photoresponse of the IRPD device under 2200 nm light illumination (80.2 mW cm^{-2}) at zero bias.

was simulated by using finite-difference time-domain (FDTD). **Figure 6**a compares the absorption curve of both PdSe$_2$/planar Ge wafer and PdSe$_2$/GeNCs array. Obviously, one can easily find that the PdSe$_2$/GeNCs array has a stronger absorption in the range from 1.0 to 1.7 µm, in good consistence with the experimental results (Figure 6b). Such a distinction in absorption is also verified by electric field energy density distributions of both structures shown in Figure 6c–e, in which obvious reflection of the incident 1550 nm light was observed on the PdSe$_2$/planar wafer structure, while the majority of the incident IR was confined by the GeNCs array. Specifically, the hot spot with relatively high electric field is about 1.5 µm away from PdSe$_2$/GeNCs interface. Without doubt, this unique optical phenomenon, usually termed as light trapping effect,[45,46] can lead to more efficient harvesting of photons, which will lead to a relatively high photocurrent in comparison with PdSe$_2$/planar Ge structure (Figure 6f). Therefore, it is highly profitable for the IR photoelectric conversion process.

To check the possibility of the current device for recording image information, which is very important in optical areas such as cameras and fax machines, we then study the imaging sensing ability using the setup shown **Figure 7**a. Since the image was recorded by individual device, an automatic displacement platform controlled

the hybrid IRPD can be readily repeated between on or off states. From a single normalized cycle of the photoresponse curve in Figure 5b, the rise and fall times are determined to be 26.43 and 38.51 µs, respectively. By deducing the relationship between relative balance (($V_{max} - V_{min})/V_{max}$) as a function of frequency in Figure 5c, the f_{3db} bandwidth is extrapolated to be ≈21 kHz.[42] From the analysis of noise spectral density in Figure 5d, the noise level per unit bandwidth (1 Hz) of the PdSe$_2$/GeNCs array IRPD was deduced to be 8.13 pA Hz$^{-1/2}$. Thereby, the specific detectivity under 1550 nm illumination was calculated to be 1.45×10^{11} Jones (please see the Supporting Information for detailed calculation process).

Table 1 lists the R, D^*, on/off ratio, τ_r/τ_f of the present IRPD and other PdSe$_2$ or Ge based IRPDs. Comprehensive comparison of these key parameters finds that our PdSe$_2$/GeNCs hybrid array IRPD is comparable to existing commercial IRPDs based on germanium. Although the specific detectivity is slightly lower than that of graphene/Ge nanoneedles array,[43] the responsivity is better than other IRPDs devices composed of graphene/Ge wafer,[34] PdSe$_2$/Si wafer,[37] graphene/Ge nanoneedles array, and graphene/Ge nanowires.[44]

In order to shed light on the relatively good performance of the above IRPD, the optical property of the hybrid structure
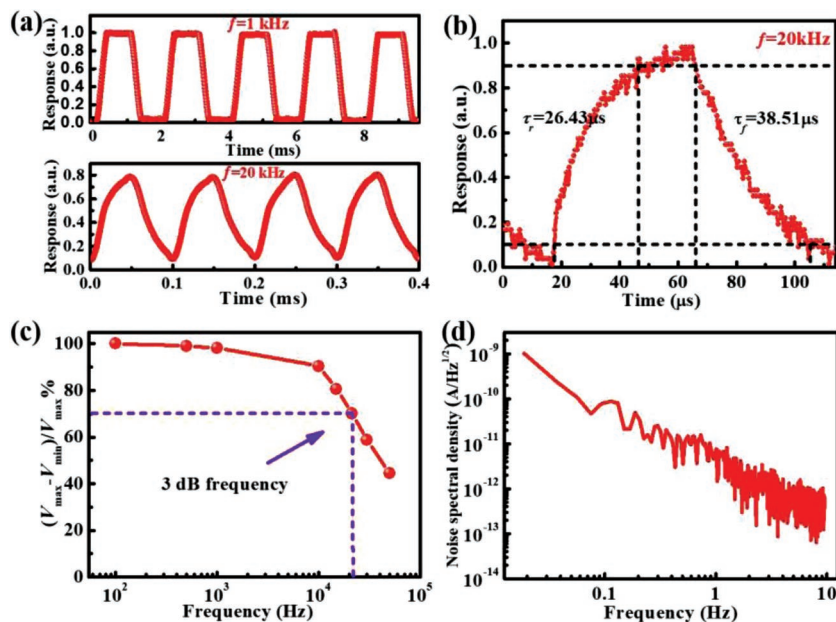

Figure 5. a) Photoresponse of the device to repeatable NIR light with a frequency of 1 k and 20 kHz. b) A single normalized cycle measured at 20 kHz for determining both rise time (τ_r) and fall time (τ_f). c) The relative balance ($V_{max} - V_{min})/V_{max}$ versus switching frequency, showing a 3 dB cutoff frequency of 21 kHz. d) Analysis of noise spectral density of the device with the dark current noise using Fourier transform.

Table 1. Comparison of key parameter of the present IRPD and other similar devices.

Device structure	R [mA W^{-1}]	D* [Jones]	τ_r/τ_f [μs]	Wavelength	Ref.
PdSe$_2$/Ge nanocones	530.2	1.45×10^{11}	25.4/38.5	1550 nm	Our work
Graphene/Ge nanoneedles	92	3.57×10^{11}	22/50	1550 nm	[39]
Graphene/Ge wafer	51.8	1.38×10^{10}	23/108	1550 nm	[35]
Ge nanowire	/	/	0.2/1 s	1550 nm	[40]
PdSe$_2$/Si wafer	≈0.37	1.2×10^{10}	38/44	1550 nm	[33]
Commercial (Ge-FDG03)	850	≈10^{11}	0.6/0.6	1550 nm	
Commercial (Ge-FDG10 × 10)	950	≈10^{11}	10/10	1550 nm	

by software-programmed computer was used. The channel current of each pixel was measured and then incorporated into a 2D contrast map. Figure 7b demonstrates the imaged English word "F" projected to image sensor: Only the area projected by the 1550 nm shows photocurrent of around 3 μA, while the rest area only has a relatively dark current. Although the uniformity of the photoresponse in the different area still needs to be improved, it clear that the word can be easily distinguished from the background, indicative of the reliable imaging capability of the hybrid structure device.

3. Conclusion

In summary, we have developed a responsive IRPD by transferring GeNCs array with a layer of PdSe$_2$ thin film, which is

obtained by a simple selenization method. The as-fabricated PdSe$_2$/GeNCs hybrid heterojunction displays apparent photovoltaic characteristics when illuminated by 1550 nm light, which can allow the hybrid device to detect IR without external power supply. It was further found that the PdSe$_2$/GeNCs hybrid based IRPD exhibited high sensitivity to 1350, 1550, and 1650 nm illumination with excellent stability and reproducibility. The responsivity and EQE was as high as 530.2 mA W^{-1} and 42.4%, respectively. This relatively good device performance according to FDTD calculation can be ascribed to the strong light trapping effect of GeNCs array. It is also observed that the hybrid structure based device exhibited an extra sensitivity to IR with wavelength longer than 2 μm. With the assistance of the automatic displacement system, our individual PdSe$_2$/GeNCs hybrid IRPD can also record the simple "F" image produced by 1550 nm. These results suggest that the
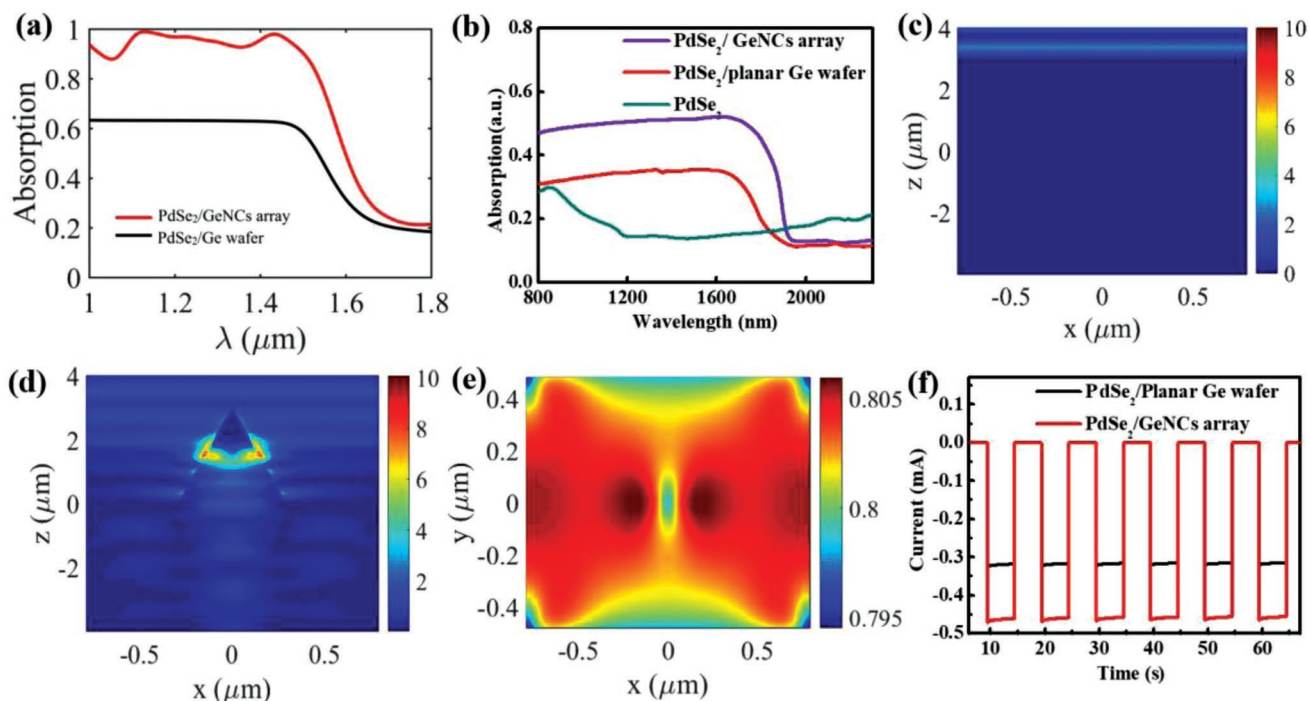

Figure 6. a) Simulated absorption curves of both PdSe$_2$/planar Ge and PdSe$_2$/GeNCs array devices. b) Experimental absorption spectra of both PdSe$_2$/planar Ge and PdSe$_2$/GeNCs array devices. Simulated electric field density distribution of c) PdSe$_2$/planar Ge and d,e) the PdSe$_2$/GeNCs array, under 1550 nm illumination. f) Photoresponse of the PdSe$_2$/GeNC array and PdSe$_2$/Ge wafer heterojunction under 1550 nm.
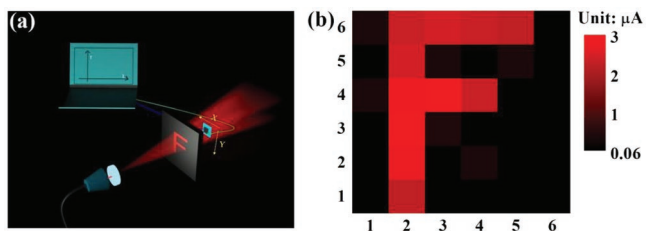
Figure 7. a) Schematic diagram of the measurement for the 1550 nm infrared image sensing application. b) The corresponding 2D current mapping of image "F" under 1550 nm illumination.

present PdSe$_2$/GeNCs hybrid device structure may find potential application in future optoelectronic systems.

4. Experimental Section

Materials Synthesis and Characterization: The PdSe$_2$ film was synthesized by a straightforward selenization approach. Briefly, a SiO$_2$/Si substrate deposited with 8 nm Pd film via an electron beam evaporator was placed at the center zone of the furnace and elemental selenium (Se) powder (99.99%) was put on the upstream side. What is more, a mixed gas of Ar and H$_2$ (50 sccm) was used as carrier and protective gas. The selenium powder was then heated to 630 K for 2 h to selenize the Pd film. The GeNNs array was obtained by a noble metal-catalyzed HF etching method. In brief, a clear n-type (100) Ge wafer pretreated sequentially by acetone, ethanol, deionized water, and a diluted HF solution was loaded with a close-packed monolayer PS (900 nm) spheres by a slow-pulling method. The as-assembled close-packed PS layer was then transformed into a nonclose-packed geometry through a reactive ion etching process, during which oxygen plasma was used, and the flow rate, pressure, and radio frequency power were kept at 20 sccm, 5 Pa, and 20 W, respectively. After coating of 20 nm silver, the Ge wafer was then immersed into a mixed solution composed of deionized water, H$_2$O$_2$, and HF (the concentrations of H$_2$O$_2$ and HF were 0.2 and 4.8 M, respectively) for 20 min. The morphology and EDS of PdSe$_2$, GeNCs array was characterized by field-emission scanning electron microscopy (FESEM, SIRION 200 FEG). The topography of PdSe$_2$ film was recorded using an AFM (Benyuan Nanotech Com, CSPM-4000). The structure of PdSe$_2$ film was analyzed by Raman spectrometer (Horiba Jobin Yvon, LabRAM HR800) and X-ray diffractometer (Rigaku D/max-rB).

Device Fabrication and Characterization: To construct the PdSe$_2$/GeNCs heterojunction photodetector, the as-selenized PdSe$_2$ film was spin coated with polymethylmethacrylate (PMMA), followed by immersion into NaOH solution (4 M) to remove the underlying SiO$_2$/Si and deionized water to remove residual ions. Afterward, the GeNCs array which was predeposited with 300 nm thick HfO$_2$ film was immersed into the deionized water, and then slowly uplifted to transfer the PdSe$_2$ films on Ge surface. Finally, after removal of PMMA with acetone, a layer of multilayered graphene was transferred on to the PdSe$_2$ layer, on which silver paste was directly put onto. The electrical measurements of the PdSe$_2$/GeNCs array heterojunction were tested using a semiconductor characterization system (Keithley 2400). The testing illuminations were NIR laser diodes with wavelengths of 1300 nm (Thorlabs, M1300L3), 1550 nm (Thorlabs, M1550L3), 1650 nm (Thorlabs, M1650L3), and 2200 nm (Thorlabs, MDL-H-2200). During the optoelectronic study, the device was shined by different light sources. To explore the response speed, a home-assembled setup composed of laser diode driven by function generator and a GHz oscilloscope (Tektronix, TDS2012B) were explored.

Theoretical Simulation: FDTD method was utilized to calculate the absorption spectra and electrical field distribution for this structure. During simulation, structural parameters of the model were extracted from the SEM image of the experimental sample, which are $P_x = 1.58$ μm,

$P_y = 0.96$ μm, $H = 3$ μm, $R = 0.58$ μm, and $t = 20$ nm, respectively. Here, P_x, P_y, H, D, and t denote the x- and y-direction period, height and bottom diameter of the Ge cone, and thickness of PbSe$_2$ film, respectively. The dielectric constant of Ge[43] and PbSe$_2$[44] was chosen.

Supporting Information

Supporting Information is available from the Wiley Online Library or from the author.

Conflict of Interest

The authors declare no conflict of interest.

[1] A. Pospischil, M. Humer, M. M. Furchi, D. Bachmann, R. Guider, T. Fromhzrz, T. Mueller, *Nat. Photonics* **2013**, *7*, 892.

[2] C. Xie, Y. Wang, Z. X. Zhang, D. Wang, L. B. Luo, *Nano Today* **2018**, *19*, 41.

[3] I. Goykhman, U. Sassi, B. Desiatov, N. Mazurki, S. Millna, D. der fazio, A. Eiden, J. Khurgin, J. Shappir, U. Levy, A. C. Ferrari, *Nano Lett.* **2016**, *16*, 3005.

[4] A. L. M. Reddy, A. Srivastava, S. R. Gowda, H. Gullapalli, M. Dubey, P. M. Ajayan, *ACS Nano* **2010**, *4*, 6337.

[5] E. J. Yoo, J. Kim, E. Hosono, H. S. Zhou, T. Kudo, I. Honma, *Nano Lett.* **2008**, *8*, 2277.

[6] S. Gumyantsev, G. X. Liu, M. S. Shur, R. A. Potyrailo, *Nano Lett.* **2012**, *12*, 2294.

[7] C. H. Lu, H. H. Yang, C. L. Zhu, X. Chen, G. N. Chen, *Angew. Chem., Int. Ed.* **2009**, *48*, 4785.

[8] X. T. Gan, R. J. Shiue, Y. D. Gao, I. Meric, T. F. Heinz, K. Shepard, J. Hone, S. Assefa, D. Englund, *Nat. Photonics* **2013**, *7*, 883.

[9] J. L. Xu, X. L. Li, Y. Z. Wu, X. P. Hao, J. L. He, K. J. Yang, *Opt. Lett.* **2011**, *36*, 1948.

[10] P. A. George, J. Strait, J. Dawlaty, S. Shivaraman, M. Chandrashekhar, F. Rana, M. G. Spencer, *Nano Lett.* **2008**, *8*, 4248.

[11] K. S. Novoselov, V. I. Falko, L. Colombo, P. R. Gellert, M. G. Schwab, K. Kim, *Nature* **2012**, *490*, 192.

[12] T. Ohta, A. Bostwick, T. Seyller, K. Horn, E. Rotenberg, *Science* **2006**, *313*, 951.

[13] L. K. Li, Y. J. Yu, G. J. Ye, Q. Q. Ge, X. D. Ou, H. Wu, D. L. Feng, X. H. Chen, Y. B. Zhang, *Nat. Nanotechnol.* **2014**, *9*, 372.

[14] J. S. Qiao, X. H. Kong, Z. X. Hu, F. Yang, W. Ji, *Nat. Commun.* **2014**, *5*, 4475.

[15] S. L. Zhang, Z. Yan, Y. F. Li, Z. F. Chen, H. B. Zeng, *Angew. Chem.* **2015**, *127*, 3155.

[16] J. P. Ji, X. F. Song, J. Z. Liu, Z. Yan, C. X. Huo, S. L. Zhang, M. Su, L. Liao, W. H. Wang, Z. H. Ni, Y. F. Hao, H. B. Zeng, *Nat. Commun.* **2016**, *7*, 13352.

[17] P. Vogt, P. D. Padova, C. Quaresima, J. Avila, E. Frantzeskakis, M. C. Asensio, A. Resta, B. Ealet, G. L. Lay, *Phys. Rev. Lett.* **2012**, *108*, 155501.

[18] M. S. Long, A. Y. Cao, P. Wang, H. Xia, C. Ott, C. Pan, Y. J. Fu, E. F. Liu, X. S. Chen, W. Lu, T. Nilges, J. B. Xu, X. M. Wang, W. D. Hu, F. Miao, *Sci. Adv.* **2017**, *3*, e1700589.

[19] B. J. Feng, Z. J. Ding, S. Meng, Y. G. Yao, X. Y. He, P. Cheng, L. Chen, K. H. Wu, *Nano Lett.* **2012**, *12*, 3507.

[20] R. D. Mahyavanshi, G. Kalita, A. Ranade, P. Desai, M. Kondo, T. Dewa, M. Tanemura, *IEEE Trans. Electron Devices* **2018**, *65*, 4434.

[21] R. Zhuo, D. Wu, Y. Wang, E. Wu, C. Jia, Z. Shi, T. Xu, Y. Tian, X. Li, *J. Mater. Chem. C* **2018**, *6*, 10982.

[22] F. H. L. Koppens, T. Mueller, P. Avouris, A. C. Ferrari, M. S. Vitiello, M. Polini, *Nat. Nanotechnol.* **2014**, *9*, 780.

[23] C. Xie, C. Mak, X. M. Tao, F. Yan, *Adv. Funct. Mater.* **2017**, *27*, 1603886.

[24] A. Gupta, T. Sakthivel, S. Seal, *Prog. Mater. Sci.* **2015**, *73*, 44.

[25] Z. X. Zhang, L. H. Zeng, X. W. Tong, Y. Gao, C. Xie, Y. H. Tsang, L. B. Luo, Y. C. Wu, *J. Phys. Chem. Lett.* **2018**, *9*, 1185.

[26] L. H. Zeng, S. H. Lin, Z. J. Li, Z. X. Zhang, T. F. Zhang, C. Xie, C. H. Mak, Y. Chai, S. P. Lau, L. B. Luo, Y. H. Tsang, *Adv. Funct. Mater.* **2018**, *28*, 1705970.

[27] D. Wu, Y. Wang, L. H. Zeng, C. Jia, E. Wu, Z. Shi, Y. Tian, X. J. Li, Y. H. Tsang, *ACS Photonics* **2018**, *5*, 3820.

[28] X. C. Yu, P. Yu, D. Wu, B. Singh, Q. S. Zeng, H. Lin, W. Zhou, J. H. Lin, K. Suenaga, Z. Liu, Q. J. Wang, *Nat. Commun.* **2018**, *9*, 1545.

[29] Y. D. Zhao, J. S. Qiao, Z. H. Yu, P. Yu, K. Xu, S. P. Lau, W. Zhou, Z. Liu, X. R. Wang, W. Ji, Y. Chai, *Adv. Mater.* **2017**, *29*, 1604230.

[30] Y. L. Wang, L. F. Li, W. Yao, S. R. Song, J. T. Sun, J. B. Pan, X. Ren, C. Li, E. Okunishi, Y. Q. Wang, E. Y. Wang, Y. Shao, Y. Y. Zhang, H. T. Yang, E. F. Schwier, H. Iwasawa, K. Shimada, M. Taniguchi, Z. H. Cheng, S. Y. Zhou, S. X. Du, S. J. Pennycook, S. T. Pantelides, H. J. Gao, *Nano Lett.* **2015**, *15*, 4013.

[31] W. L. Chow, P. Yu, F. C. Liu, J. H. Hong, X. L. Wang, Q. S. Zeng, C. H. Hsu, C. Zhu, J. D. Zhou, X. W. Wang, J. Xia, J. X. Yan, Y. Chen, D. Wu, T. Yu, Z. X. Shen, H. Lin, C. H. Jin, B. K. Tay, Z. Liu, *Adv. Mater.* **2017**, *29*, 1602969.

[32] A. D. Oyedele, S. Z. Yang, L. B. Liang, A. A. Puretzky, K. Wang, J. J. Zhang, P. Yu, P. R. Pudasaini, A. W. Ghosh, Z. Liu, C. M. Rouleau, B. G. Sumpter, M. F. Chisholm, W. Zhou, P. D. Rack, D. B. Geohegan, K. Xiao, *J. Am. Chem. Soc.* **2017**, *139*, 14090.

[33] L. H. Zeng, D. Wu, S. H. Lin, C. Xie, H. Y. Yuan, W. Lu, S. P. Lau, Y. Chai, L. B. Luo, Z. J. Li, Y. H. Tsang, *Adv. Funct. Mater.* **2019**, *29*, 1806878.

[34] E. Li, D. F. Wang, F. Fan, R. Z. Zhang, Y. Y. Zhang, G. Li, J. H. Mao, Y. L. Wang, X. Lin, S. X. Du, H. J. Gao, *Nano Res.* **2018**, *11*, 5858.

[35] L. H. Zeng, M. Z. Wang, H. Hu, B. Nie, Y. Q. Yu, C. Y. Wu, L. Wang, J. G. Hu, C. Xie, F. X. Liang, L. B. Luo, *ACS Appl. Mater. Interfaces* **2013**, *5*, 9362.

[36] Q. S. Lv, F. g. Yan, X. Wei, K. Y. Wang, *Adv. Opt. Mater.* **2018**, *6*, 1700490.

[37] C. Xie, X. T. Lu, X. W. Tong, Z. X. Zhang, F. X. Liang, L. Liang, L. B. Luo, Y. C. Wu, *Adv. Funct. Mater.* **2019**, *29*, 1806006.

[38] W. Y. Kong, G. A. Wu, K. Y. Wang, T. F. Zhang, Y. F. Zou, D. D. Wang, L. B. Luo, *Adv. Mater.* **2016**, *28*, 10725.

[39] Z. F. Chen, Z. Z. Cheng, J. Q. Wang, X. Wan, C. Shu, H. K. Tsang, H. P. Ho, J. B. Xu, *Adv. Opt. Mater.* **2015**, *3*, 1207.

[40] T. Mueller, F. X. Nia, P. Avouris, *Nat. Photonics* **2010**, *4*, 297.

[41] C. H. Liu, Y. C. Chang, T. B. Norris, Z. H. Zhong, *Nat. Nanotechnol.* **2014**, *9*, 273.

[42] L. Wang, J. S. Jie, Z. B. Shao, Q. Zhang, X. H. Zhang, Y. M. Wang, Z. Sun, S. T. Lee, *Adv. Funct. Mater.* **2015**, *25*, 2910.

[43] R. Lu, C. W. Ge, Y. F. Zou, K. Zheng, D. D. Wang, T. F. Zhang, L. B. Luo, *Laser Photonics Rev.* **2016**, *10*, 595.

[44] C. Y. Yan, N. Singh, H. Cai, C. L. Gan, P. S. Lee, *ACS Appl. Mater. Interfaces* **2010**, *2*, 1794.

[45] K. X. Wang, Z. F. Yu, V. Liu, Y. Cui, S. H. Fan, *Nano Lett.* **2012**, *12*, 1616.

[46] S. Jeong, E. C. Garnett, S. Wang, Z. F. Yu, S. H. Fan, M. L. Brongersma, M. D. McGehee, Y. Cui, *Nano Lett.* **2012**, *12*, 2971.